The Thesis Committee for Brent Joel Pafford
Certifies that this is the approved version of the following thesis:

Investigation of Magnetohydrodynamic Plasma Actuators for Aerodynamic Flow Control

APPROVED BY
SUPERVISING COMMITTEE:

Supervisor:

Jayant Sirohi

Laxminarayan L. Raja

Investigation of Magnetohydrodynamic Plasma Actuators for Aerodynamic Flow Control

by

Brent Joel Pafford, B.S.

Thesis

Presented to the Faculty of the Graduate School of

The University of Texas at Austin

in Partial Fulfillment

of the Requirements

for the Degree of

Master of Science in Engineering

The University of Texas at Austin

May 2013

Dedicated to past, present, and future family.

Acknowledgements

First I would like to show my gratitude to my wife Amber for her support and encouragement, without which I would not be where I am today. I am greatly beholden to my supervisor, Professor Jayant Sirohi for his support and encouragement over the last few years. I have taken great pleasure in working with Professor Sirohi and the majority of my research would not have been possible without his help. I would also like to Professor Laxminarayan L. Raja for his guidance, serving as a co-supervisor, and collaboration on the current work. I want to thank Dwayne Surls and Francis Stefani for their guidance and expertise during the initial design phase of my research. Finally I would like to thank Young-Joon Choi for his assistance with creating computer programs to analyze the experimental data.

Abstract

Investigation of Magnetohydrodynamic Plasma Actuators for Aerodynamic Flow Control

Brent Joel Pafford, M.S.E

The University of Texas at Austin, 2013

Supervisor: Jayant Sirohi

This thesis describes the analysis, fabrication and testing of a novel magnetohydrodynamic plasma actuator for aerodynamic flow control, specifically, retreating blade stall. A magnetohydrodynamic plasma actuator is comprised of two parallel rail electrodes embedded chord-wise on the upper surface of an airfoil. A pulse forming network generates a low-voltage, high-current repetitive pulsed arc. Self-induced electromagnetic fields force the pulsed arc along the length of the rail electrodes at high velocities, transferring momentum to the surrounding air, creating a high-velocity pulsed air wall jet. A systematic experimental investigation of the effect of plasma actuators on the surrounding air is conducted in stagnant air conditions to gain an understanding of the physical characteristics. These characteristics include voltage and current measurements, pulsed arc velocity measurements, and high speed video imaging. The results show typical pulsed arc velocities of about 100 m/s can be induced with discharge energies of about 300 J per pulse.

Additional experimental studies are conducted to quantify the performance of the pulsed arc for potential use in subsonic flow control applications. To gain an estimate of the momentum transferred from the pulsed arc to the surrounding air the plasma actuator is placed in a subsonic open-circuit wind tunnel at a Reynolds number of 4.5×10^5. The induced velocity of the pulsed wall jet is measured using a Laser Doppler Anemometer. The measurements show that the pulsed arc creates a high-velocity pulsed wall jet that extends 40 mm above the airfoils surface and has an induced velocity of 15 m/s greater than the unaltered air flow over the airfoil, with peak velocities of 32 m/s.

The magnetohydrodynamic plasma actuator proved to induce velocities an order of magnitude greater than the velocities attained by current state-of-the-art plasma actuators. Moreover, the RailPAc is found to posses the potential for alleviation of retreating blade stall. Future work will include experiments to gain a detailed understanding of the improvements to the static stall angle, the optimal actuator geometry, excitation duty cycle, magnetic field augmentation, and behavior of the plasma armature at high Mach/Reynolds numbers. Particle Image Velocimetry (PIV) will be utilized to improve the induced flow velocity measurements acquired with the LDA.

Table of Contents

List of Figures

Chapter 1

Introduction

1.1 MOTIVATION

Future high performance rotary-wing vehicles are expected to feature significant increased cruise speed and maneuverability, increased operating range, a growth in payload capability, and a substantial increase in mission efficiency. However, some critical limitations pose challenges to attaining these goals. Static stall on the airfoils limits the maximum blade loading, and hence the maximum thrust that can be generated by the rotor. This not only limits the maximum payload or cargo capacity of a helicopter, but also limits maneuverability. Furthermore, conventional helicopters are limited in forward flight by compressibility effects on the advancing blade, as well as stall on the retreating blade [1]. While compressibility effects can be alleviated by slowing the rotor in forward flight, this increases the stall on the retreating side. Therefore, retreating blade stall poses a fundamental limitation on the maximum speed of a helicopter.

Retreating blade stall is characterized by the occurrence of dynamic stall once per revolution over the retreating side of the rotor disk. This manifests itself as a large increase in vibration, coinciding with the onset of pitching moment stall. The onset of stall is typically expressed in terms of a stall boundary, which defines a decrease in maximum allowable blade loading as a function of increasing advance ratio. The conventional approach to address this issue has been to appropriately size the main rotor solidity so that it has sufficient stall margin during extreme flight conditions. Passive methods to alleviate stall have also been examined, to include, leading edge slats [2] and steady flow control methods such as air injection [3] and suction [4]. While passive

devices are beneficial in terms of stall alleviation, they can have an adverse effect on the advancing side of the rotor disk in terms of increased drag.

Studies have been conducted to show how unsteady excitation can create low level periodic forcing to modulate the formation of vortices in a separating flow. These techniques include Directed Synthetic Jet (DSJ) and Periodic Flow Modulation (PFM) [5] (Figure 1.1).

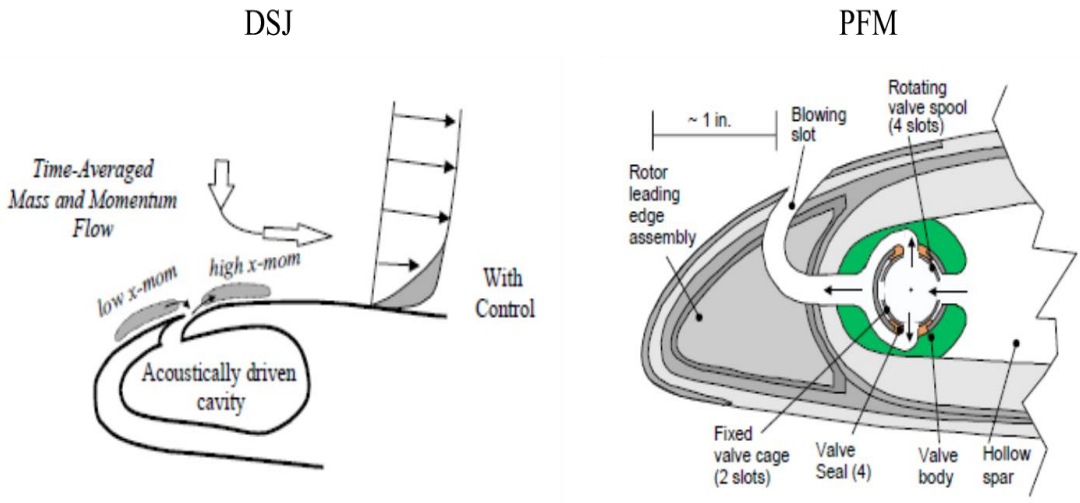

Figure 1.1: Schematic of a Directed Synthetic Jet (DSJ) and Periodic Flow Modulation (PFM) Devices. The figure is reproduced from Lorber and McCormick (2000)

The Directed Synthetic Jet applies acoustic streaming to form a synthetic jet with an exit neck optimized for separation control. The curved neck allows low momentum fluid to be ingested during the suction phase and high momentum fluid to be ejected during the blowing phase, energizing the boundary layer. Periodic flow modulation uses two concentric slotted cylinders to periodically inject flow into the boundary layer creating unsteady excitation. The advantage of these concepts is that they can be actuated once per revolution over the retreating side, thus eliminating them where they are not

required. An analytical study of the effectiveness of these methods concluded that they can result in an increase in blade loading of 3%-10% at a given constant rotor aerodynamic power [6]. In spite of the advantages of these concepts, their practical implementation is very challenging. The active devices require mechanically complex, compact, high power actuation mechanisms that must be sufficiently robust to withstand the highly vibratory and centrifugal environment in a rotor blade. Likewise, supplying sufficient quantity of air into the rotating frame for blowing applications can also be challenging, and the small cavities necessary for synthetic jets may not survive in a dusty, realistic operational environment.

Chapter 2

State of the Art

2.1 PLASMA ACTUATORS FOR FLOW CONTROL

Plasma actuators are suitable for aerodynamic flow control because they conform to aerodynamic surfaces and contain no moving parts. The concept of plasma actuators for active flow control has been demonstrated to be an effective method to generate unsteady vortical distributions [7]. The two main types of plasma actuators are electrohydrodynamic (EHD) and magnetohydrodynamic (MHD). EHD plasma actuators rely on forces generated by electrostatic fields that create a hydrostatic pressure near a dielectric material. The pressure gradient moves ionized air across the electrostatic field and imparts momentum to the surrounding air. MHD plasma actuators rely on electromagnetic fields that induce a current in a moving fluid which imparts a force on the fluid. The force on the ionized fluid propels it at high speeds and imparts momentum to the surrounding air.

2.1.1 EHD Actuators

EHD plasma actuators consist of two electrodes separated by a dielectric material and flush mounted on the upper surface of an airfoil. The actuators rely on EHD forces created by the current between the electrodes at voltages on the order of several Kilo Volts (kV). Applicable high voltage supplied to the electrodes causes the air in their vicinity to weakly ionize. The ionized air (plasma) in the presence of the electric field gradient, produced by the electrodes, results in a body force vector acting on the external flow that can induce steady or unsteady velocity components [8]. As a result, flow can be

entrained into the boundary layer and separation can be delayed. Although the voltage required is high, the current drawn is low (order of milliamps). There are four basic types of plasma actuators [9]: DC surface corona, AC dielectric barrier discharge (DBD), sliding discharge and wall jet.

Out of these types, DBD actuators are the easiest to construct, the most robust, and have a high control authority. The mechanical configuration of the DBD plasma actuator is shown in Figure 2.1 [10].

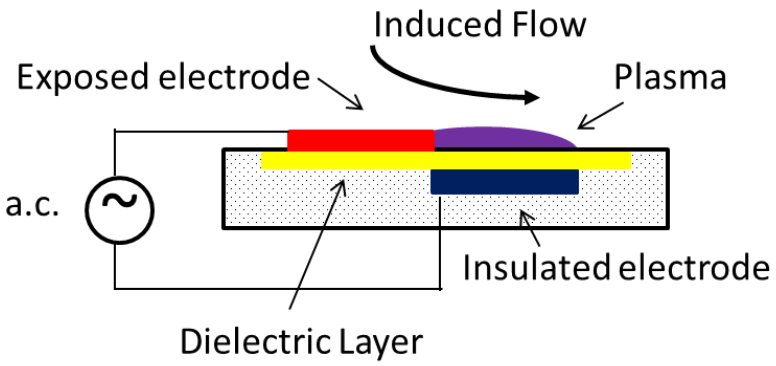

Figure 2.1: Schematic of a DBD actuator. The figure is reproduced from Enloe and McLaughlin (2004)

The DBD plasma actuator consists of a pair of thin electrodes, usually copper foil tape or small gauge copper wire, arranged span-wise on an aerodynamic surface. One electrode is exposed to the air, while the other is encapsulated in a dielectric, usually Kapton polyimide tape. When an AC voltage of 5 to 10 kV at a frequency between 4 to 10 kHz is applied to the electrodes, the unaided eye sees an apparently diffuse plasma discharge. The appearance of the plasma is accompanied by a momentum coupling into the surrounding air. This momentum coupling can be effective in substantially altering

the flow of air over the actuator surface and is equally effective in introducing a flow in still air.

The effectiveness of these devices has been demonstrated on a variety of applications including flow separation control [9, 11], dynamic stall alleviation [12], and smart wind turbine blades [13]. The DBD plasma actuators have demonstrated improved control authority compared to trailing-edge flaps for control of an unmanned air vehicle [14] and their performance has been experimentally investigated [15]. At a Reynolds number of 4.12×10^5 the DBD actuators are ideally suited for application on Unmanned Aerial Systems (UAS). However, sufficient control authority at the Mach numbers and Reynolds numbers representative of full-scale rotary-wing vehicles has not been demonstrated to date, in spite of ongoing research over the past decade.

2.1.2 MHD Actuators

MHD plasma actuators consist of two parallel electrodes flush mounted on the upper surface of an airfoil. The actuators rely on the current (***J***) passing through the ionized air (plasma field) created between the electrodes inducing a magnetic field (***B***), which generates a strong Lorentz force (***JxB***) on the plasma field. The plasma field is accelerated by the Lorentz force transferring momentum to the surrounding air creating a high-velocity pulsed air wall jet. As a result, flow near the surface of an airfoil can be periodically accelerated and delay boundary layer separation. Contrary to EHD actuators MHD actuators operate at low voltages (~V) and high current levels (~kA).

Chapter 3

Present Approach

3.1 RAIL PLASMA ACTUATOR CONCEPT

The innovative MHD plasma actuator explored in the present approach is the Rail Plasma Actuator, named RailPAc. The RailPAc is capable of inducing flow velocities in quiescent air and increasing the free stream velocity of airflow over the surface of an airfoil. This potentially makes RailPAcs relevant for full-scale aerodynamic applications.

3.1.1 Physical principles

The operating principle of the RailPAc is similar to that of the electromagnetic rail gun [16]. The RailPAc repetitively discharges a free moving plasma arc (called a "plasma armature") that relies on self-induced magnetic fields to move at high velocities along a pair of rail electrodes. Figure 3.1 shows a schematic of the parallel copper electrodes, called "rails", embedded chord-wise in an airfoil.

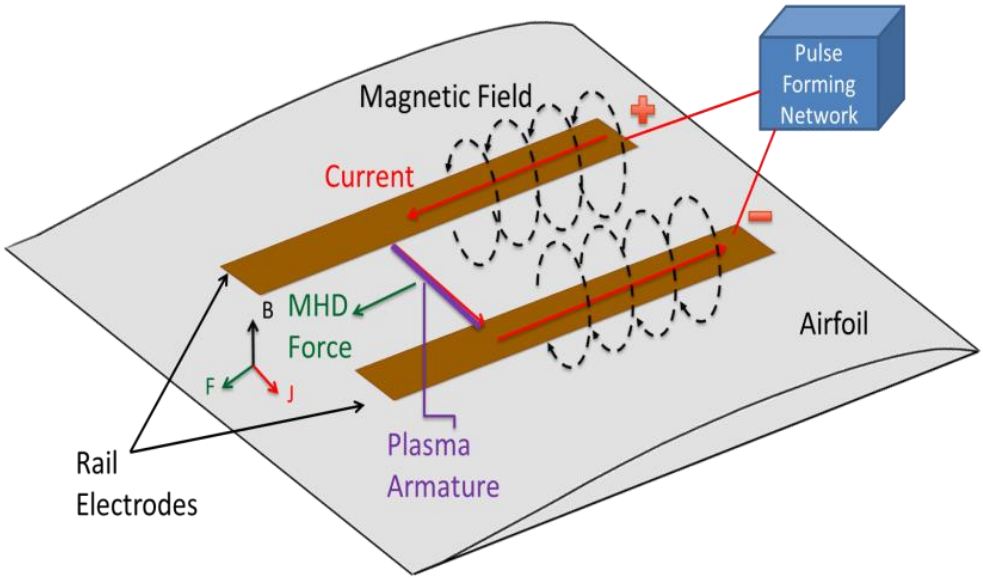

Figure 3.1: Schematic of the Rail Plasma Actuator (RailPAc)

A pulse forming network connected to the rails initiates a plasma discharge close to the leading edge of the rails. The plasma arc, or "armature" can be sustained at a low voltage (~100 V) and a large current (~1 kA) for a short period of time (~ 1 ms) depending on the physical characteristics of the pulse forming network.

The current loop formed by the rails and plasma armature (Figure 3.1) induces a net magnetic field $\boldsymbol{B}$ perpendicular to the plane of the rails. Interaction between the magnetic field and the current carried by the plasma armature produces a strong magnetohydrodynamic Lorentz force which accelerates the plasma armature along the rails.

The armature reaches a terminal velocity determined by the Lorentz force and the aerodynamic drag on the armature. At atmospheric pressure conditions, the armature behaves like a solid body in motion [17] and therefore aerodynamic drag on the armature is a measure of the momentum transferred to the surrounding air. In essence, the

armature motion induces a velocity in the surrounding air through compression at the leading end of the armature and entrainment effects on the trailing end of the armature. Activation of the RailPAc accelerates neutral air flow in vicinity of the RailPAc and possesses the potential to delay boundary layer separation.

3.2 PRELIMINARY INVESTIGATIONS OF THE ELECTRICAL PROPERTIES AND PERFORMANCE OF THE RAILPAC IN QUIESCENT AIR

The influence of various parameters on the magnitude and performance of the plasma armature is investigated on a proof-of-concept bench-scale RailPAc. The effect of the RailPAc's electrical properties on the plasma armature is explored by measuring the voltage across the rails and the current from the pulse forming network. A comprehensive study of the performance of the plasma armature as a function of the capacitance and charge voltage of the pulse forming network is conducted. Additionally, high-speed images of the plasma armature are captured to quantify the physical characteristics and the speed of the plasma armature. The goal of the bench-scale trials is to demonstrate the ability of the RailPAc to generate induce a wall jet in stagnant air conditions and utilize the experimental data to optimize the pulse forming network for increased plasma armature performance.

3.3 INVESTIGATIONS OF AN AIRFOIL EMBEDDED RAILPAC PERFORMANCE IN A WIND TUNNEL

The transfer of momentum from the plasma armature to the surrounding air is examined on a RailPAc embedded in a two-dimensional wind tunnel test article. The velocity of the airflow over the top of an airfoil is measured utilizing a Laser Doppler Anemometer (LDA). Tests to measure the velocity of the pulsed wall jet are conducted

at specific spatial locations in vicinity of the airfoil surface to determine the size and magnitude of the effects of the plasma armature on the surrounding air. The goal of the wind tunnel experiments is to discern the pulsed wall jet velocity profile as a function of chord location and height above the airfoil surface.

Chapter 4

Experimental Setup

The RailPAc and the pulse forming network are both designed and fabricated in house at the University of Texas. Therefore, every aspect of the RailPAc is tested and studied. Initial experiments are employed to optimize the pulse forming network to the RailPAc. Additional experiments are conducted on a proof-of-concept bench-scale RailPAc in stagnant atmospheric air conditions to measure the electrical properties of the actuator and capture high-speed imaging of the plasma armature quantifying the physical characteristics of the RailPAc. Experiments performed on the RailPAc embedded in the wind tunnel test article measure the induced flow velocities created by the plasma armature utilizing a Laser Doppler Anemometer (LDA). This chapter explores the design of the pulse forming network, the two initiation systems used in conjunction with the pulse forming network, the bench-scale prototype, the two-dimensional test article, and the systematic experiments.

4.1 Pulse Forming Network

A Xantrex XHR 600-1.7 direct current (D.C.) power supply is used to charge a capacitor bank to different charge voltages (V_c) from 150 V to 250 V. The capacitor bank is comprised of six parallel Sprague Powerlytic 36DX electrolytic capacitors with a total capacitance of 21 milifarads (mF) and a rated maximum charge voltage of 450 V. The capacitor bank discharges through a 15 microhenry (μH) air core inductor. The plasma armature can be initiated by a switch activated exploding fuse wire or by a spark

generating trigger circuit. The trigger circuit is utilized to sustain repetitive pulses at a desired frequency.

4.1.1 Exploding Fuse Wire

A thin gage 5 mil. aluminum fuse wire is used to bridge the rails. An open switch between the rails and the pulse forming network ensures that the voltage potential between the rails remains at zero while the capacitor bank charges. This allows the capacitor bank to charge to the voltage required to create and sustain a plasma armature. Figure 4.1 shows the RailPAc separated from the pulse forming network by the trigger switch.

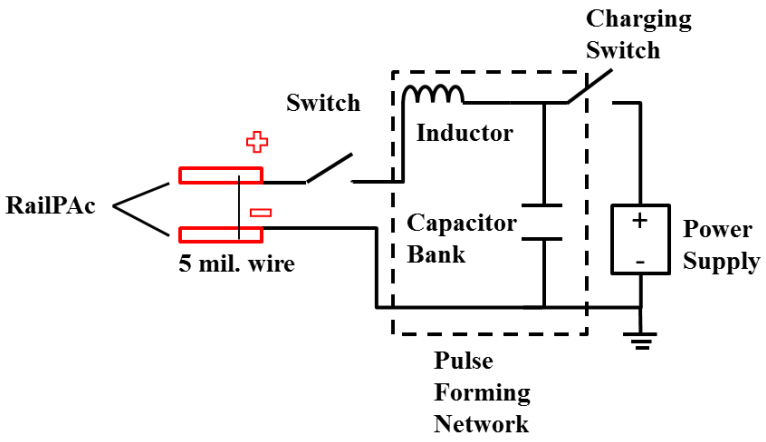

Figure 4.1: Switch activated exploding wire initiation pulse forming network

Once the switch is closed the pulse forming network is connected to the rails through the electrical leads and creates the plasma armature from a tiny metal vapor plasma kernel produced by the exploding fuse wire. The plasma armature is then

accelerated along the rails. This initiation technique only provides a single pulse per wire explosion and after every discharge a new wire must be fixed to the rails.

4.1.2 Trigger Circuit

The positive rail and the negative rail are connected directly to the capacitor bank bringing the rails to the voltage of the capacitor bank (Figure 4.2). The trigger circuit initiates a localized corona-like discharge across a small perturbation on one of the rails. The corona discharge crosses the gap between the rails completing the circuit and quickly transforming into a plasma armature.

The capacitance and inductance of the pulse forming network is tailored to the plasma armature transit time and the length of the rails. The trigger circuit allows the plasma armature discharge to be repeated with a frequency that can be tailored to a specific unsteady flow phenomenon. Due to the continuous motion of the plasma armature along the rails and the short transit time, there are no adverse thermal effects on the underlying structure from the plasma discharges.

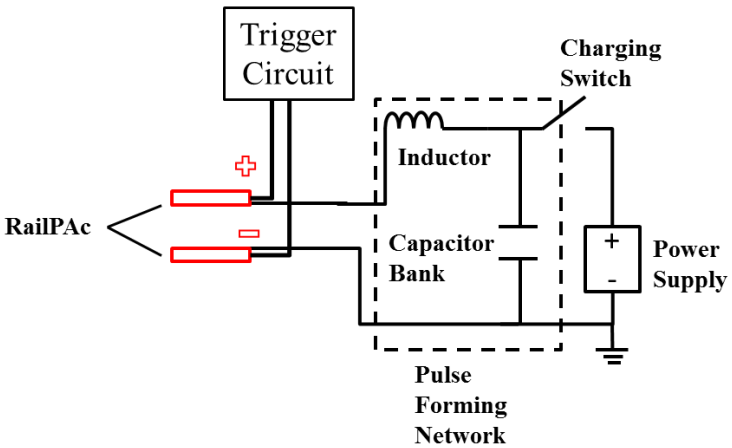

Figure 4.2: Spark activated RailPAc pulse forming network

4.2 PROOF-OF-CONCEPT BENCH-SCALE PROTOTYPE

A proof-of-concept bench-scale prototype is constructed to qualitatively evaluate the operation of the RailPAc and to investigate methods of arc initiation (Figure 4.3). Two parallel 6 inch long, 0.4 inch wide and 1/32 inch thick copper electrode strips (rails) are flush mounted on a dielectric surface with a spacing of 0.5 inches. The electrodes are connected to a power supply that drives a large current on the order of kilo amps (kA) at relatively low voltages on the order of 100 volts (V) for a short duration of time, approximately 2 milliseconds (ms).

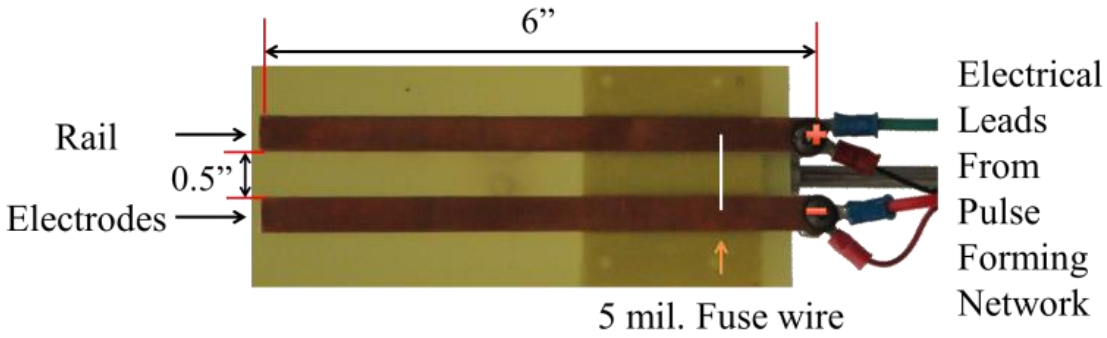

Figure 4.3: Proof-of-concept bench-scale prototype RailP**A**c device

Figure 4.3 shows the positive electrode connected to the negative electrode through the 5 mil. fuse wire at the right end of the RailPAc (breech end). The plasma armature travels from the breech to the muzzle (left end).

4.3 WIND TUNNEL TEST ARTICLE

Wind tunnel tests were performed to evaluate the induced velocity profile of the RailPAc over an aerodynamic surface. A RailPAc is embedded in a two-dimensional wind tunnel test article (Figure 4.4). The test article is a S5010 airfoil with a span of 32.25 inches and a chord of 14.5 inches. The RailPAc is comprised of two identical

copper rail electrodes that are 0.4 inches wide and 12 inches long. The rails are flush mounted on a dielectric surface starting at 7% chord and separated by a gap of 0.4 inches. Utilizing the pulse forming network in conjunction with the trigger circuit, the plasma armature is initiated at the leading edge (section 4.1.2), of the rails and travels in the chord-wise direction.

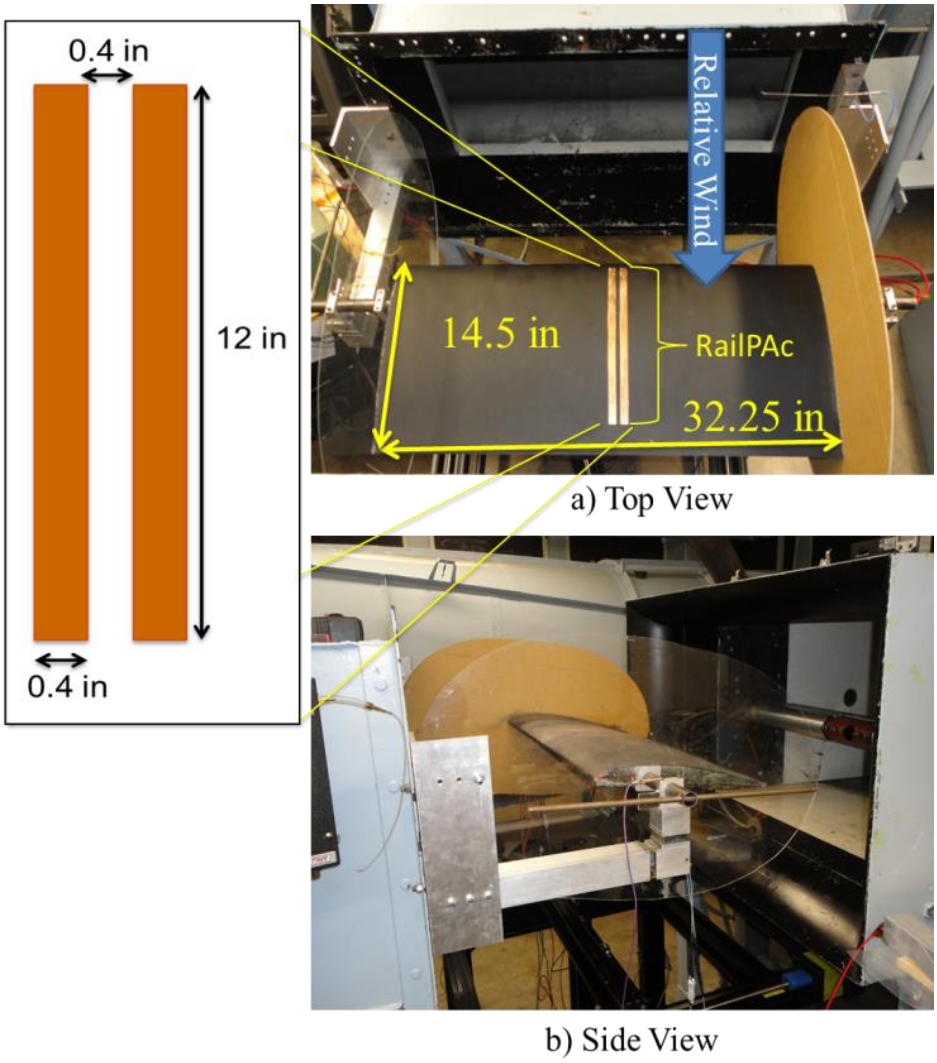

Figure 4.4: Wind tunnel test article consisting of RailPAc embedded in a 2D airfoil section

The copper rails conform to the airfoil profile without altering the shape or structural integrity and have a negligible weight penalty. When the actuators are not in use the airfoil operates as a passive unaltered airfoil, because the rails are mounted smoothly on the surface of a rotor blade. Therefore, the addition of the RailPAc has no adverse effects on the performance of the rotor blade.

4.4 Plasma Armature Velocity Measurements

A Vision Research high-speed digital camera is used to capture video of the armature motion. The digital images are used to measure the velocity of the plasma armature and the spatial extent of the plasma armature. Top-down digital images of the plasma armature are acquired at a rate of 76,000 frames per second with a window size of 256 x 64 pixels. Frontal view images are acquired at a rate of 47,000 frames per second with a window size of 512 x 256 pixels. To increase the precision of the measurement the camera's aperture is placed at the minimum diaphragm opening, corresponding to an f-stop of 24, and a 10 mil. Mylar film lens is placed on the outside of the lens to act as a neutral-density filter. This procedure is conducted to eliminate the bright superheated air that surrounds the plasma armature. The exploding wire initiation pulse forming network (section 4.1.1) is used for all high-speed imaging experiments and the wind tunnel experiments are conducted with the trigger circuit initiation pulse forming network (section 4.1.2).

4.5 Flow Visualization

The vision Research high-speed digital camera is also used to capture and display a flow visualization of the induced flow. The momentum transferred from the plasma

armature to the surrounding air is demonstrated using KEVLAR tufts placed 1 inch above the rails from the point of initiation to 6 inches past the trailing-edge of the rails (Figure 4.5). The tufts hang perpendicular to the RailPAc in quiescent atmospheric air conditions and will be used to visually depict the extent of the induced pulsed wall jet created by the plasma armature.

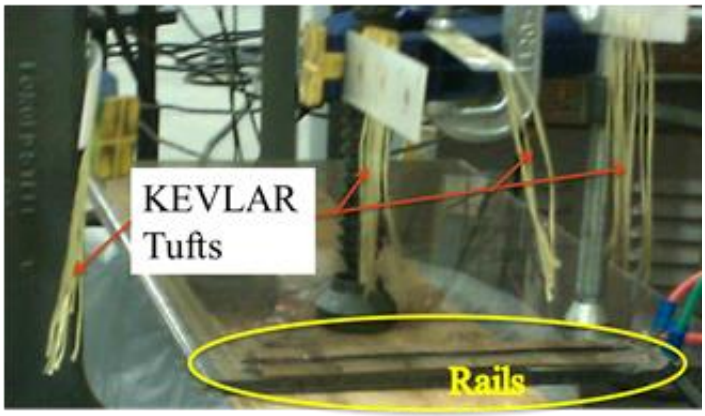

Figure 4.5: Bench-scale RailPAc prototype flow visualization experimental set up

4.6 Electrical Characteristics

All electrical signals are acquired and observed using a Tektronix 4 channel oscilloscope. The current is measured using a Powertek – Rogowski Current Waveform Transducer. The Rogowski Transducer is secured around the positive electrical lead between the pulse forming network to the positive rail. The transducer measures the rate at which the charge flows through the transducer coil with respect to time.

The voltage is measured using a differential voltage probe coupled to the muzzle of the rails with the electrical leads. The voltage probe records the voltage potential across the rails with respect to time.

4.7 Induced Flow Measurements

The wind tunnel test article is mounted in a sub-sonic open circuit wind tunnel and secured by two force balances in the lift and drag directions (Figure 4.4(b)). A Dantec Dynamics Laser Doppler Anemometer (LDA) is used to capture point-wise measurements of the flow velocity profile of the air immediately above the RailPAc at multiple free stream velocities. The LDA transmitting and receiving optics are mounted below the test article on a graduated mechanical traverse, capable of moving the sensing head in the chord-wise (x), span-wise (z), and normal (y) directions. Therefore, the test article is placed upside down in the wind tunnel (Figure 4.6) at a zero degree angle of attack. A V_c of 250 V was used for all LDA experiments.

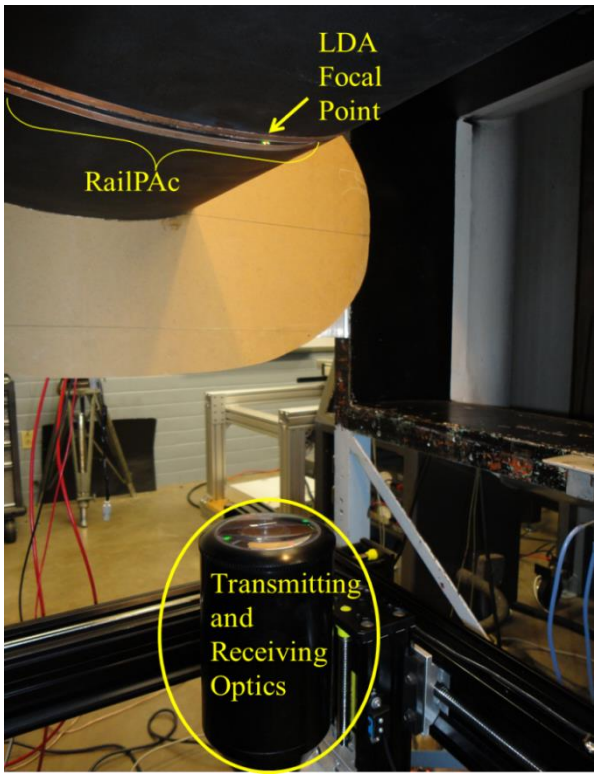

Figure 4.6: LDA induced flow velocity experimental set up

The focal point of the LDA is fixed in the center of the channel formed by the rails of the RailPAc and traverses in the chord-wise direction (x) from the leading edge to the trailing edge acquiring data every 25 mm. While stationary in the x direction the LDA is moved vertically (y) away from the surface of the airfoil to 45 mm above the airfoil surface. Figure 4.7 shows the measurement grid. All results are presented with the airfoil correct side up.

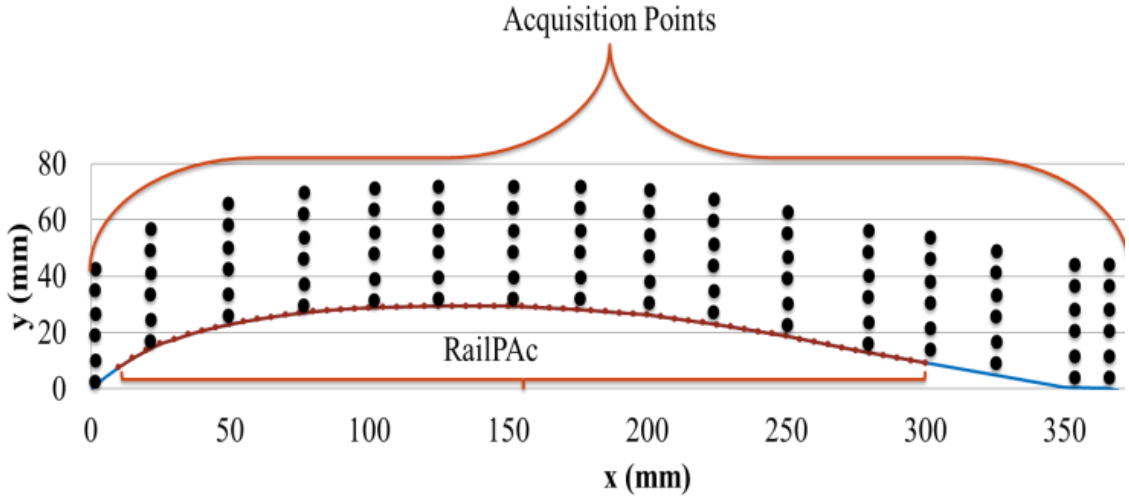

Figure 4.7: LDA induced flow velocity acquisition points above the RailPAc wind tunnel test article

Starting at the leading edge velocity measurements are acquired at 9 different locations in the y direction from the surface outward. The LDA measures the velocity of every seed particle that transitions through the focal point of the LDA. The seed particles are generated with a Rosco Fog Machine that seeds the wind tunnel with a dense water-based aerosol fluid. The LDA records the arrival time of the seed particle to the focal point and the transition time of the seed particle through the 1mm beam width at the focal point. The individual velocities of seed particles flowing over the passive airfoil (RailPAc turned off) are calculated along with the mean velocity (U_{mean}) of the seed

particles captured during a 25 second sampling window. After the passive signal is stored the test is repeated at the same location with the RailPAc turned on. The RailPAc discharges 10 plasma armatures at a frequency of 1.25 Hertz (Hz) during the 25 second sampling window. The velocity signal with RailPAc on is compared to the passive signal by calculating the average of multiple velocity peaks produced by the RailPAc.

The open test section of the wind tunnel allows a large portion of the seed particles to escape reducing the fog density. Because the LDA operates on the random arrival time of the seed particles the sampling rate is random and at times very slow compared to the pulse duration of the armature. Due to the random sampling rate and the short interval of the plasma armature (~2 ms) not all of the plasma armature transits are captured and recorded. Therefore, to properly analyze the results the LDA processor is linked to the pulse forming network through a common reference trigger system. Using the common reference trigger all velocity peaks in the LDA signal are directly correlated with the discharge of a plasma armature. Depending on the spatial location of the LDA focal point peak velocities occur every 2 – 9 ms after plasma armature discharge. The delay in the peak velocity is created by the 2.25 ms transition time of the plasma armature and the time it takes for the armature to transfer momentum to the surrounding flow.

Chapter 5

Results and discussion

5.1 Plasma Armature Velocity Measurements

Filtered high-speed imaging is used to observe the relationship between capacitor charge voltage (V_c) and plasma armature velocity. Figure 5.1 shows the high-speed imaging of the RailPac discharge for an initial V_c of 250 V.

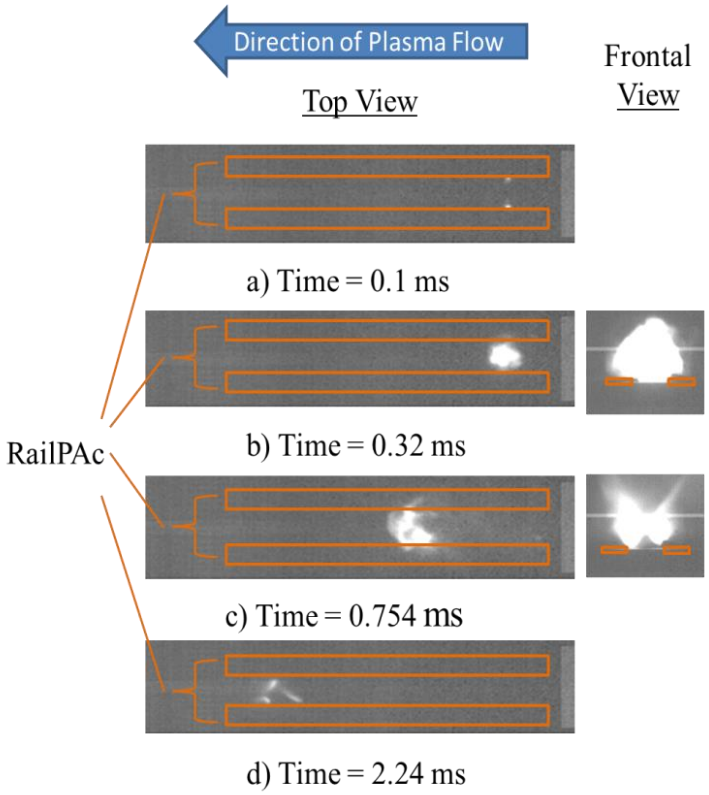

Figure 5.1: Filtered high-speed video of plasma armature motion. Top view images of the armature motion at 0.1, 0.32, 0.754, and 2.24 ms after discharge are shown. Frontal view images of the armature at 0.32 and 0.754 ms illustrate the vertical extent of the arc from the surface. The red rectangles indicate the outline of the rails. V_c equal to 250 V

The filtered top-down view shows the plasma armature at quiescent atmospheric conditions from the initiation (Figure 5.1(a)) at a time of 0.1 ms traversing from right to left maintaining consistent contact with the rails until 2.24 ms when the arc begins to extinguish (Figure 5.1(d)). Between the time of 0.32 ms and 0.754 ms the intensity of the armature has grown significantly, corresponding to a current of 1.75 kA and 3.25 kA, respectfully. The frontal view of the armature is also shown at a time of 0.32 ms and 0.754 ms. The frontal view shows that the area of the armature exceeds 1 square centimeter. The frontal view also shows that at 0.754 ms the plasma armature is traveling on top of the rails and is not localized between the rails. This allows the rails to be flush mounted on an airfoil and removes the need for the rails to be slightly elevated above the surface of the airfoil.

The high-speed video was used to calculate the transient velocity of the plasma armature by measuring the distance traveled between frames.

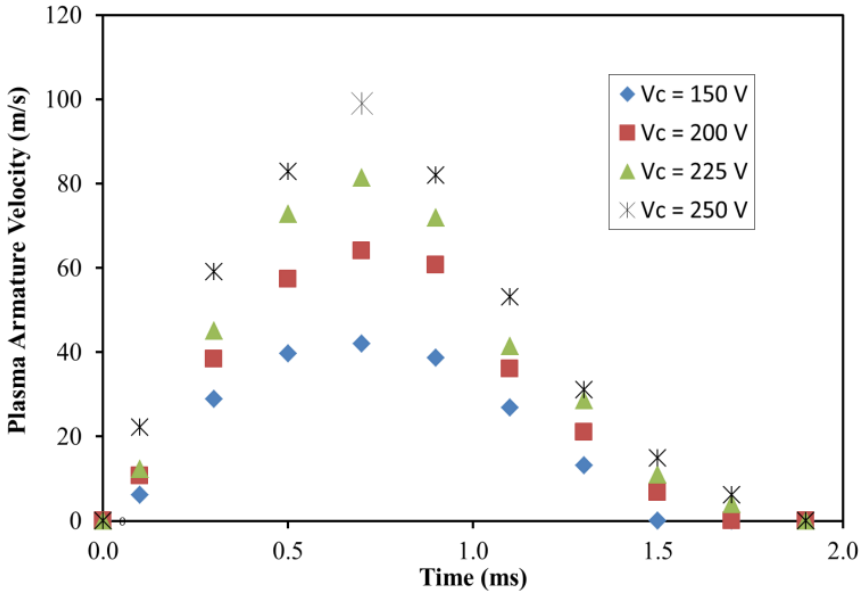

Figure 5.2: Plasma armature velocity as a function of time and V_c

Figure 5.2 is a plot of the plasma armature velocity with respect to time for four initial V_c values of 150 V, 200 V, 225 V, and 250 V. Following terminal velocity all four profiles decrease to a velocity of zero. The results of the plasma armature velocity measurements show that the velocity increases to a maximum of 100 meters per second (m/s) at 0.754 ms after initiation, and then decreases to zero for a V_c of 250 V.

5.2 ELECTRICAL CHARACTERISTICS

The plasma armature current, ***J***, rapidly increases from 0 A to ~ 1 kA coinciding with an increase in the magnetic field, ***B***. The Lorentz force (***JxB***) acting on the plasma armature reaches a maximum approximately 2.5 inches from the breech (Figure 5.1(c)). As the plasma armature reaches the muzzle the current diminishes and the armature decays. Figure 5.3 depicts the transient values of the current through the rails for capacitor charge voltages of 150 V and 250 V. Comparing Figure 5.2 with Figure 5.3 shows that the velocity profile follows the transient profile of the current. This corresponds to the Lorentz force on the plasma armature. As the current increases the Lorentz force increases accelerating the plasma armature until the current reaches the maximum transient value. Following the current peak the armature begins to decelerate towards the end of the rails.

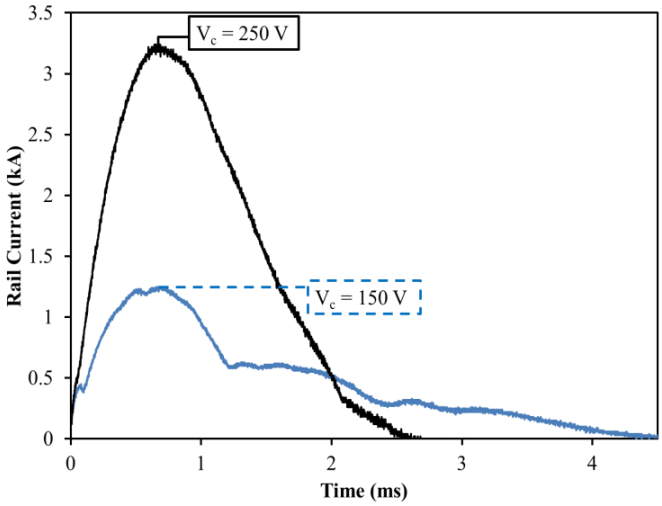

Figure 5.3: Rail current as a function of time and capacitor charge voltage

The plasma armature current increases to a maximum peak value dependent on V_c. At a charge voltage of 250 V the peak current is 3.25 kA, while the peak current at a charge voltage of 150 V is 1.25 kA. The peak current values are reached at 0.754 ms for both cases. Following the peak value, the current diminishes to zero. All current peak values occur at 0.754 ms because the transient current is only a function of the capacitance and inductance of the pulse-forming network.

The frequency of the current through the plasma armature is defined as:

$$\omega = \frac{1}{\sqrt{LC}}$$

The period of the plasma armature becomes:

$$T = \sqrt{LC}2\pi$$

Therefore, a constant inductance and capacitance yields a consistent armature pulse interval with a constant current peak time.

The plasma armature current transient, including the time of the peak current coincides with the plasma armature velocity transient in Figure 5.2. An increase in V_c causes a rise in ***J*** resulting in a stronger ***B*** field, an increase in initial acceleration, and a higher terminal velocity. Therefore the velocity of the plasma armature is coupled to current through the Lorentz Force and the aerodynamic drag acting on the armature.

The voltage across the rails for a V_c of 150 V and 250 V can be viewed in Figure 5.4. The voltage initially spikes due to the transient voltage rise across the inductor. With a V_c of 250 V a voltage spike of 400 V is observed and quickly dissipates to a steady state rail voltage of 80 V. For a Vc of 150 V the spike reaches a magnitude of 216 V and returns to a rail voltage of 60 V. Following the transient spike the voltage fluctuates until approximately 3 ms. After the plasma armature has extinguished the pulse forming network and rails remain at the steady state voltage.

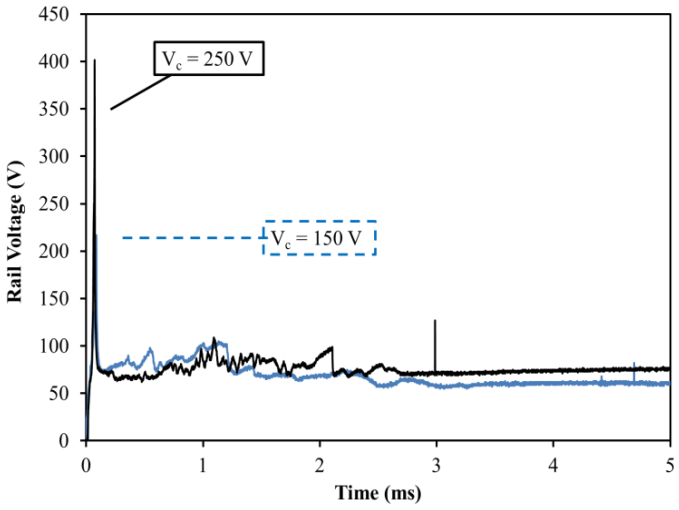

Figure 5.4: Rail voltage as a function of time and capacitor charge voltage

The plasma armature instantaneous electrical power is the product of the current through the rails and the rail voltage. Figure 5.5 shows the plasma armature instantaneous power for a V_c of 150 V and 250 V with respect to time.

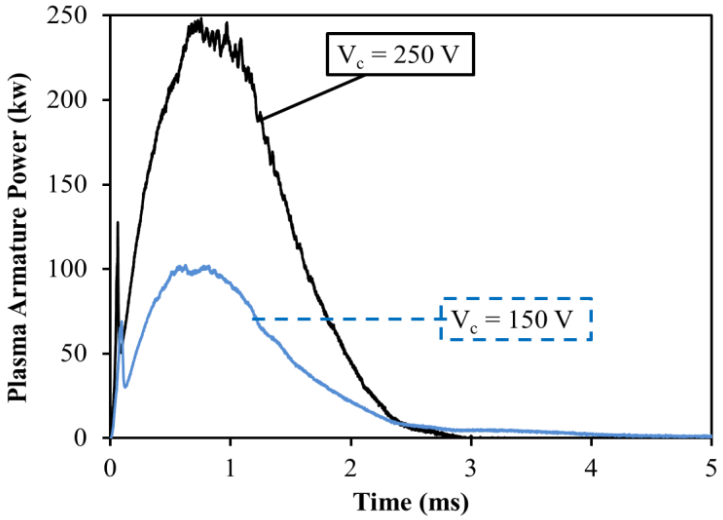

Figure 5.5: Plasma armature power as a function of time at a V_c of 150 V and 250 V

Due to the transient voltage spike through the inductor the power initially spikes to 123 kilowatts (kW) and 64 kW for a V_c of 150 V and 250 V. The peak power of 248kW, for a V_c of 250 V, and 99 kW, for a V_c of 150 V, occurs at 0.754 ms in direct correlation with the peak armature current and velocity. A time integration of the power in Figure 4.5 results in a total energy of 312 Joules (J) and 146 J at a V_c of 250 V and 150 V. Figure 5.6 shows the relationship between capacitor charge voltage and energy consumed by the plasma armature per pulse.

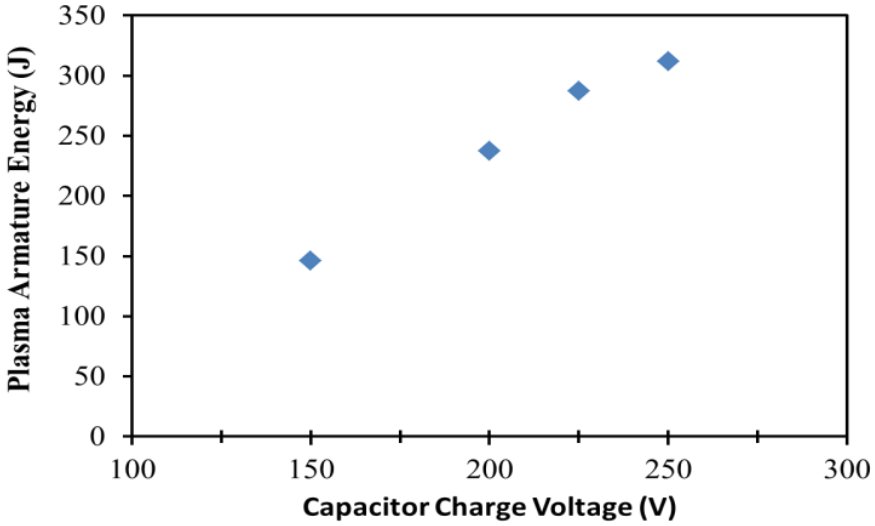

Figure 5.6: Plasma armature energy as a function of V_c

The initial energy available in the capacitor bank is found using the following equation:

$$E_{cap} = \frac{1}{2} C V_c^2$$

The stored energy in the capacitor bank is 236 J, 420 J, 532 J, and 656 J for the four initial V_c values. For the case of V_c equal to 250 V the energy available is 656 J and the energy consumed by the plasma armature is 312 J, 48% of the initial energy available in the capacitor bank. The voltage of the capacitor bank following the plasma discharge is 80 V resulting in an available energy value of 67 J. We can conclude that 30% to 40% of the initial capacitor energy is lost due to non-discharge related occurrences.

Figure 5.7 shows the relationship between the peak velocity of the plasma armature at the initial V_c values of 150 V, 200 V, 225 V, and 250 V and the energy required to sustain the plasma armature at the given V_c values.

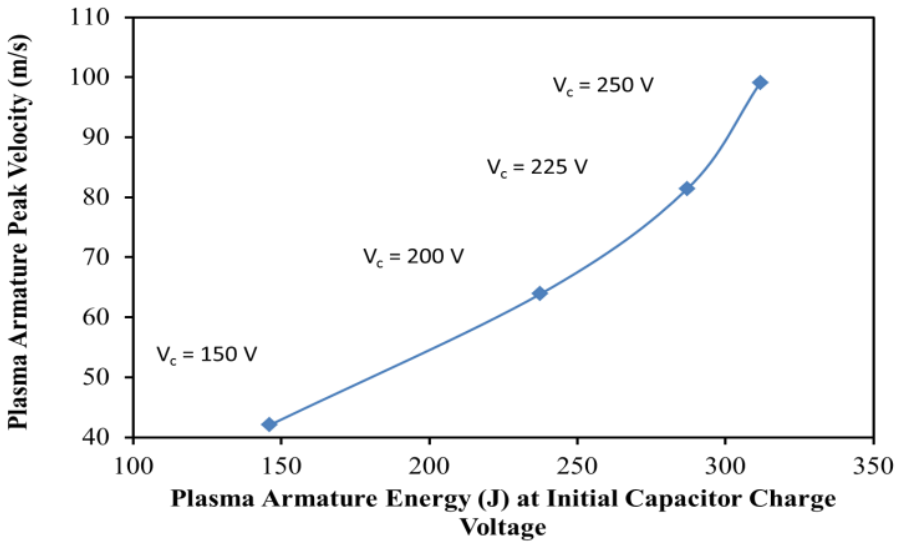

Figure 5.7: Peak plasma armature velocity as a function of plasma armature energy per pulse and V_c

Figure 5.7 shows that higher plasma armature peak velocities are achieved through greater initial stored energy in the capacitors. At the higher values of V_c an increase in plasma armature velocity is gained with reduced increases in initial capacitor charge energy. This leads to improved performance of the plasma armature with minimal change to the input power. The increase in performance is attributed to the lower plasma armature resistance at higher values of V_c. For the four initial V_c values the plasma armature resistance is 67 milliohms (mΩ), 48 mΩ, 31 mΩ, and 24 mΩ. The reduction in plasma armature resistance at higher V_c values leads to a higher plasma armature velocity.

Figure 5.8 displays the efficiency of the pulse forming network as a function of plasma armature peak velocity and V_c. At higher values of V_c the plasma armature achieves a higher peak velocity and consumes less of the initial energy available in the capacitor bank. With a V_c of 250 V the RailPAc uses 48% of the available capacitor

bank energy to drive the plasma armature compared to 62% at a V_c of 150 V. Therefore, increasing the charge voltage not only improves the speed of the plasma armature, but improves the performance and efficiency of the plasma armature as well.

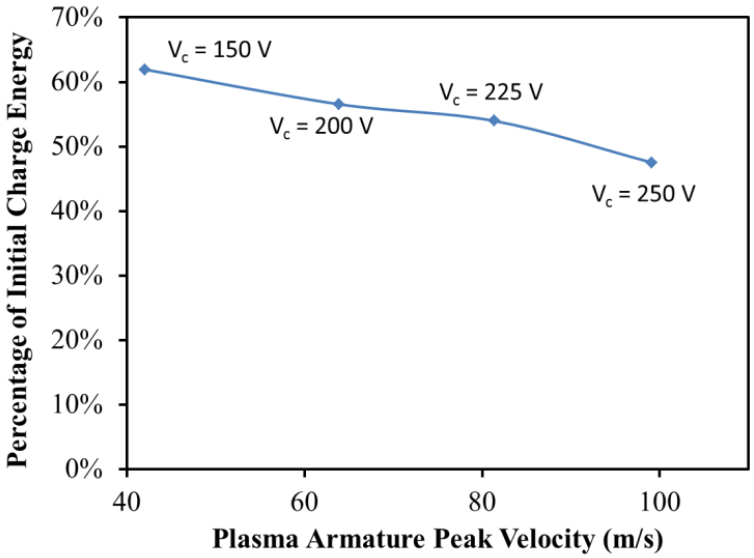

Figure 5.8: Ratio of plasma armature energy to initial capacitor bank energy as a function of plasma armature peak velocity

5.3 Flow Visualization

High-speed imaging is used to qualitatively assess the flow field induced by the plasma armature motion. Figure 5.9 shows the high-speed imaging of the induced wall jet created by a single plasma armature discharge for an initial V_c of 250 V. The flow induced by the plasma armature is observed deflecting the tufts up to 90 degrees beyond their initial vertical position.

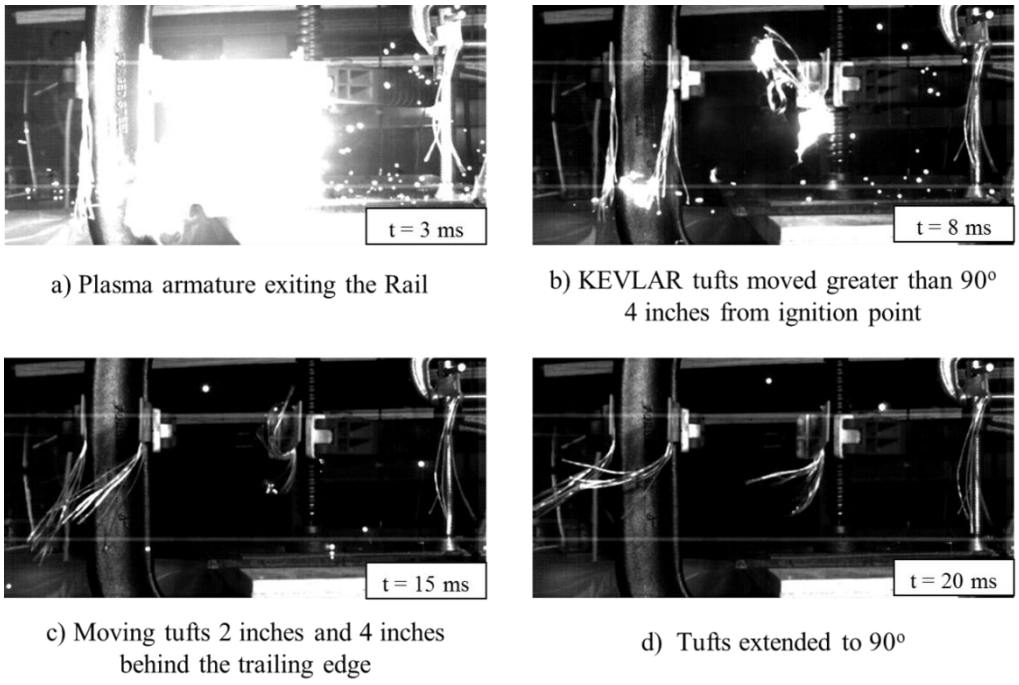

a) Plasma armature exiting the Rail

b) KEVLAR tufts moved greater than 90° 4 inches from ignition point

c) Moving tufts 2 inches and 4 inches behind the trailing edge

d) Tufts extended to 90°

Figure 5.9: High-speed video of the induced pulsed wall jet. The flow visualization images of the wall jet at 3, 8, 15, and 20 ms after discharge are shown. The side view images illustrate the vertical extent of the wall jet from the surface and demonstrates the plasma armatures ability to induce a wall jet in stagnant air.

The white flash in Figure 5.9(a) signifies the departure of the plasma armature from the RailPAc and the superheated air surrounding the RailPAc. Figure 5.9 demonstrates the ability of the plasma armature to impart momentum into the air above the RailPAc and create an induced flow that lasts in excess of 20 ms. Figure 5.9 (c & d) show the tufts located 4 and 6 inches aft of the rails experiencing the induced wall jet and move greater than 90 degrees in the direction of the flow. This motion was found to persist up to 20 ms after the initiation of the armature motion. The induced flow has the potential to provide unsteady excitation to create low level periodic forcing to modulate the formation of vortices in a separating flow preventing boundary layer separation and postponing stall.

5.4 Induced Flow Measurements

Figure 5.10 shows the LDA signal that is captured at a spatial position of 225.00 mm in the x direction and 27.84 mm in the y direction corresponding to the acquisition point 5 mm above the surface of the airfoil at 60% chord. The free stream velocity of the wind tunnel is 15.77 m/s with a resultant chord Reynolds number of 4.5 x 10^5. The signal in Figure 16 represents the velocity of 32,000 seed particles that transit the focal point of the LDA. The passive, RailPAc turned off, mean velocity (U_{mean}) of the vaporized particles is 17.02 m/s.

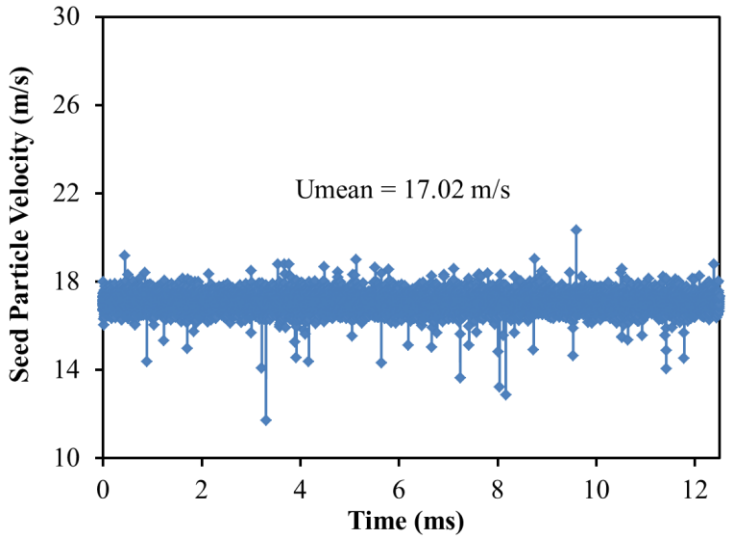

Figure 5.10: LDA measured velocity of seed (vaporized water) particles at the LDA focal point of (225 mm, 27.84 mm)

Figure 5.11 shows the coupling of the voltage signal from the capacitor bank with the velocity signal from the LDA. The sudden drop in voltage pinpoints the initiation of the plasma armature at the breech. The large spike in the LDA signal at 6.649 s is the result of the induced flow wall jet passing the focal point of the LDA.

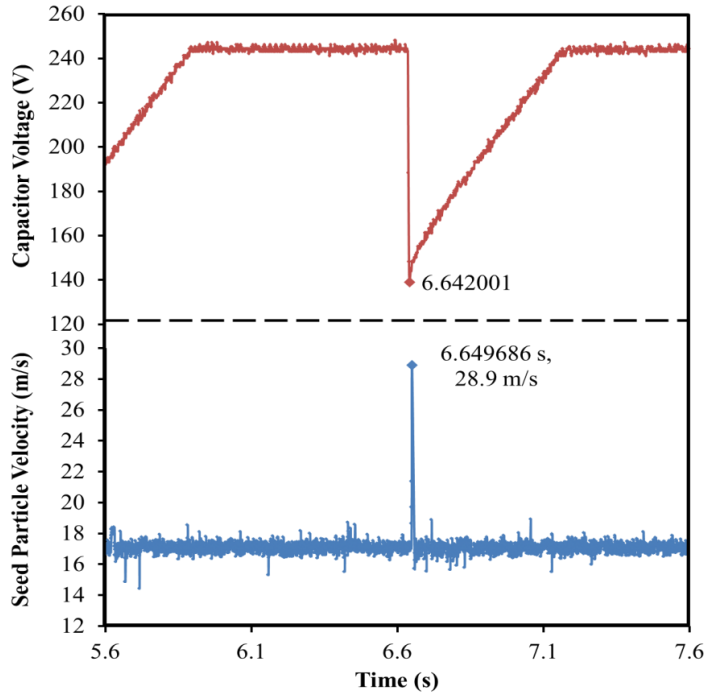

Figure 5.11: Capacitor Voltage and LDA velocity signal of water vapor particles with respect to a common reference time

The analysis of the velocity peak in Figure 5.11, compared with the mean velocity in Figure 5.10, shows that at 7.685 ms after the initiation of plasma armature there is an increase in the flow velocity from 17.02 m/s to 28.9 m/s 5 mm above the RailPAc and 225 mm aft of the leading edge (60% chord). The pulse forming network is designed to drive the plasma from the breech, located 37.25 mm aft of the leading edge (10% chord), along the rails to 223 mm aft of the leading edge (60% chord). The LDA spatial focal point was 2 mm aft of the plasma armature termination point. Given the time to travel the rails of 2.25 ms and the delay due to the entrainment effects, the induced flow created by the plasma armature on the neutral air reaches a maximum velocity at approximately 8 ms after plasma armature initiation, at this particular spatial location. Figure 5.11 shows a zoomed in view of the velocity spike at 6.6496 ms.

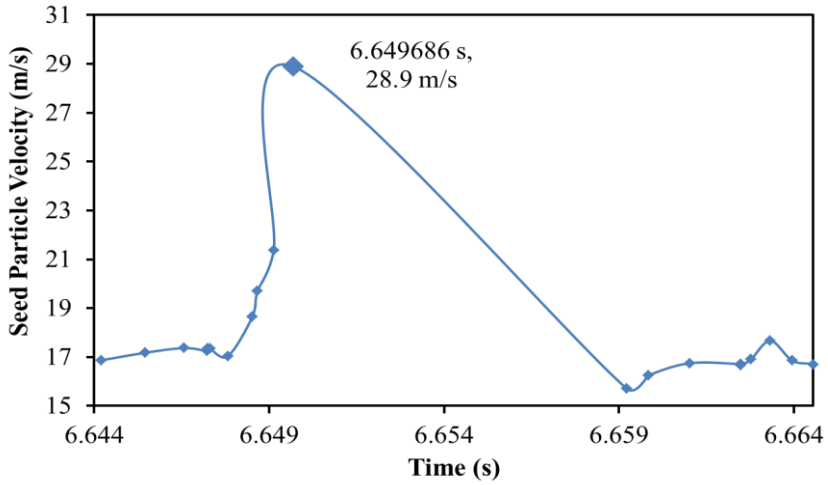

Figure 5.12: Increase in measured seed particle velocity due to plasma armature motion

In Figure 5.12 there is a rapid increase in the velocity of seed particles transitioning through the LDA focal point. Following the particle that was captured at 6.649686 s there is a 10 ms absence of seed particles due to the effects of the plasma armature on the passive air flow. The Lorentz force accelerates the plasma armature as it travels chord-wise along the rails transferring momentum into the boundary layer. The air entrained behind the plasma armature pushes the seed particles away from the LDA focal point accounting for the 10 ms absence of seed particles. This is an inherent limitation of the LDA technique because it relies on the random arrival of the seed particles.

The maximum peak seed particle velocity is measured at all spatial locations indicated in Figure 4.7. Several measurements are acquired at each point and these are averaged to yield the peak induced flow velocity. At a given chord-wise location, the peak induced flow velocity as a function of height from the airfoil surface yields the velocity profile of the induced flow. Figure 5.13 displays the velocity profile of the induced flow created by the RailPAc compared to the velocity profile of the flow over the

passive airfoil. This data is captured at 60% chord (225 mm) and approximately 7 ms after initiation of the plasma armature.

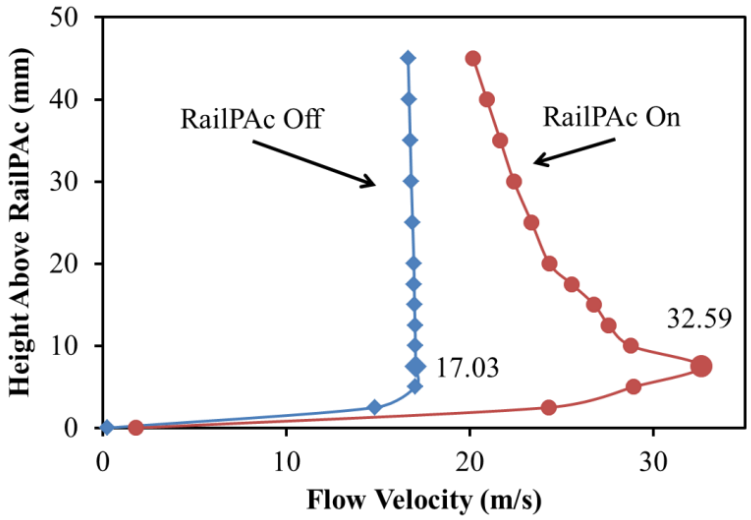

Figure 5.13: Flow velocity comparison over the test article surface at 60% chord with and without RailPAc activation

The RailPAc is observed to induce a wall jet with a peak induced flow velocity of 15.56 m/s above that of the free stream velocity. The location of the peak velocity is at 7.5 mm above the airfoil surface and the effect of the RailPAc induced flow velocity continues for 45 mm above the surface. These induced flow velocities are significantly higher than those obtained with DBD actuators and can further be increased with careful optimization of the rail geometry, pulse energy, and pulse duration. Also the RailPAc induces flow over a large volume of air, 8 times greater than the boundary layer thickness of approximately 5 mm.

To provide a greater understanding of the RailPAc's control authority, velocity profile comparisons at chord-wise locations of 15%, 47%, and 80% chord are displayed

in Figures 4.13, 4.14 and 4.15, respectively. At 15% chord (50 mm) the induced flow is greatest at 7.5 mm above the surface at 33.03 m/s (Figure 5.14). The height of the induced flow is reduced at this location because the plasma armature has not fully developed.

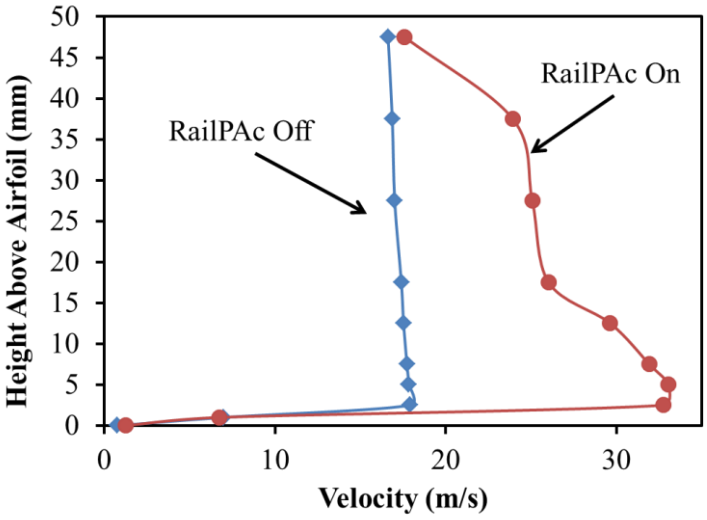

Figure 5.14: Flow velocity comparison over the test article surface at 15% chord with and without RailPAc activation

At 47% chord the induced flow wall jet has a maximum velocity of 29.58 m/s and the height of the wall jet extends to 15 mm above the surface of the RailPAc. The plasma armature is fully developed at 47% chord resulting in a taller wall jet, with respect to the airfoil surface (Figure 5.15). At 47% chord the wall jet velocity created by the plasma armature is double that of the free stream velocity of 15.77 m/s.

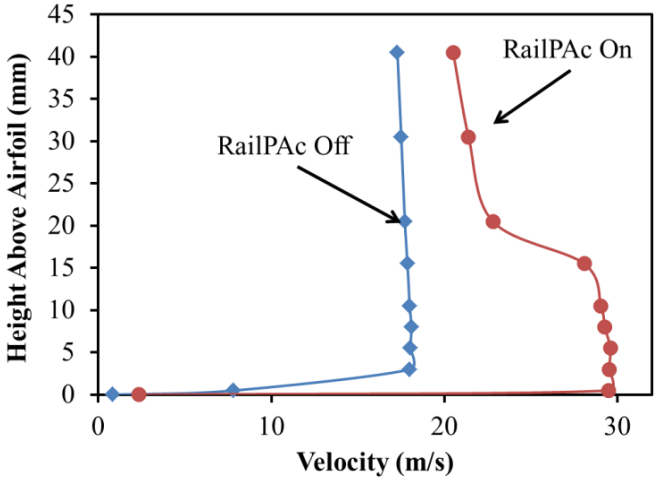

Figure 5.15: Flow velocity comparison over the test article surface at 47% chord with and without RailPAc activation

As the wall jet nears the trailing edge (80% chord) it begins to slow down because the plasma armature starts dissipating and the momentum transfer subsides. However, on average, the wall jet affected by the plasma armature is 5 m/s greater than the passive air flow over the airfoil (Figure 5.16).

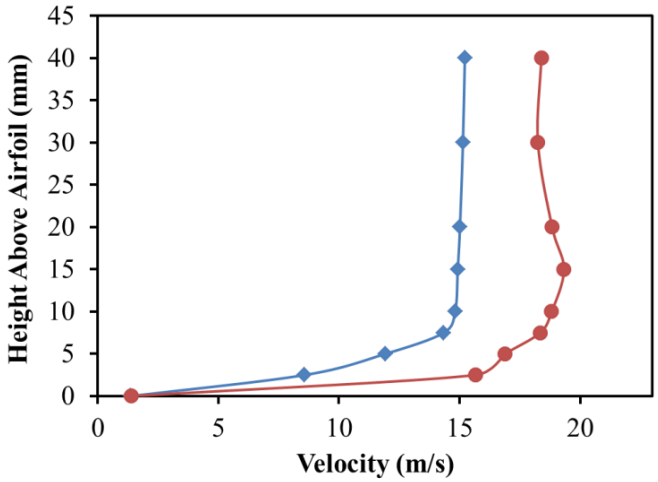

Figure 5.16: Flow velocity comparison over the test article surface at 80% chord with and without RailPAc activation

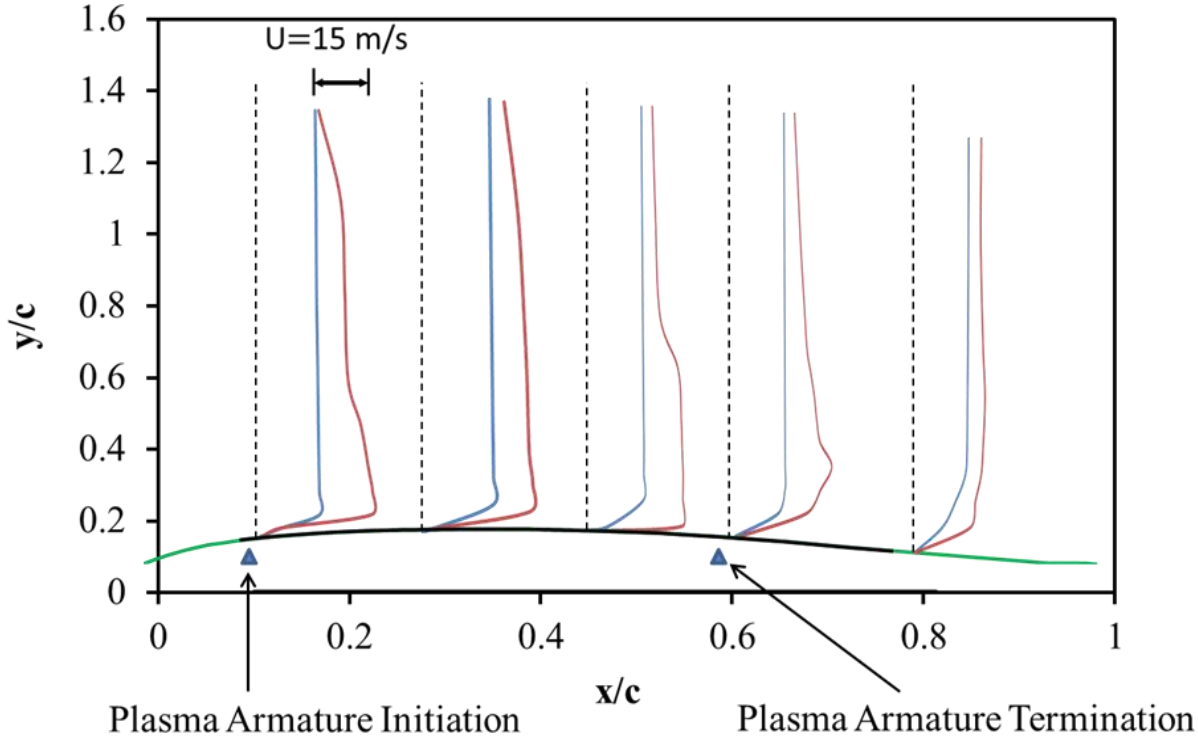

Figure 5.17: Flow velocity comparison over the test article surface with and without RailPAc activation as a function of chord location. The first velocity profile (blue line) in every group is the passive flow.

The results of the LDA velocity measurements are consolidated in Figure 5.17, which shows the velocity profile created by the plasma armature compared to the passive flow velocities as a function of chord location. From 15% chord to the trailing edge the plasma armature increases the velocity of the flow over the surface of the airfoil. From 15% to 60% chord the increase in flow velocities is 15 m/s or greater.

Chapter 6

Summary and conclusions

Magnetohydrodyamic plasma actuators were fabricated and experimentally tested in stagnant air conditions and simulated forward flight. The goal was to develop plasma actuators that could be used for aerodynamic flow control specifically to delay boundary layer seperation. The actuators called Rail Plasma Actuators or RailPAcs are comprised of a pair of rail electrodes that can be embedded on the surface of an airfoil, contain no moving parts, require no structural modification of the airfoil, and have a negligible weight penalty. A pulse forming network generates a low-voltage, high-current plasma armature that produces an induced wall jet. In conjunction with existing electrical circuits, high currents can be achieved locally at the RailPAc to propagate a plasma armature. Most importantly, an electrical failure will have no adverse effects on the airfoil, which will simply revert to a purely passive condition.

A systematic experimental investigation was conducted to define the effects of the electrical characteristics of the RailPAc on the plasma armature, utylizing a bench-scale prototype. The pulse forming network was charged to four different intial charge voltages while measuring the current, rail voltage, and plasma armature velocity during plasma armature discharge. For capacitor bank discharges with an energy output of ~100 J plasma armature velocities of ~100 m/s were observed in tranquil air using high-speed imaging. The experimental data indicated that the most efficient and best performing plamsa armature was generated with a charge voltage of 250 Volts. Results show that an increase in the charge voltage of the capacitor bank leads to a increase in the plasma armature peak velocity. Furthermore, the peak velocity of the plamsa armature is found

to be primarily dependent on the charge voltage of the capacitor bank and independent of other discharge parameters such as inductance and capacitance. An increase in charge voltage yields an increase in peak current, wchich in turn increases the $\boldsymbol{B}$ field and accelerates the plasma armature at a greater rate. Therefore, increasing the charge voltage produces an increased peak velocity of the plasma armature.

Increasing the charge voltage of the capacitor bank also increases the effeciency of the plasma armature. Increasing the charge voltage returns a rise in the current discharged from the capacitor bank with a decrease in the resistance between the plasma armature and the rails. Not only is the resistance between the rails decreased, but the plasma armature consumes less of the avaliable energy from the capacitor bank. Therefore, increasing the capacitor charge voltage increases the speed of the plasma armature and improves the efficiency of the plasma armature.

The developmental experiments conducted on the bench-scale prototype not only provided the necessary flow visualization and velocity profile of the plasma armature, but also provided a solid baseline for future experiments. Future work on the bench-scale prototype will include variations to the rail geometry, enhancement of the magnetic field, and new initiation techniques. Changing the rail geometry can lead to an increase in the volume of air effected by the plamsa armature. Enhancement or augmentation of the magnetic field in the middle of the RailPAc will lead to an increase in the peak velocity of the plasma armature. However, sufficient tests need to be conducted to determine the effects of the augmented magnetic field on the overall shape of the plasma armature. A new initiation system needs to be investigated to remove the need for a high voltage spark to complete the circuit between the rails. The high voltage spark is the most dangerous part of the circuit with regards to humans and electrical equipment.

The second phase of experimentation was conducted on a two-dimensional wind tunnel test article and validated the ability of the RailPAc to create an induced pulsed wall jet in forward flight. When placed in a sub-sonic open circuit wind tunnel at zero degrees angle of attack and a free stream velocity of 16 m/s the RailPAc demonstrated the propagation of an induced wall jet with peak velocities of 32 m/s. The RailPAc proved to induce velocities an order of magnitude greater than the velocities attained by electrohydrodynamic dielectric barrier discharge plasma actuators and provide the potential for alleviation of aerodynamic stall.

Because the wind tunnel has an open test section and the seeding of water particles was random, at high Reynolds numbers the LDA was unreliable and unable to accurately record velocity profiles. Therefore, the validity of the RailPAc at high Reynold's numbers is still unkown. Future plans for wind tunnel experiments involve using Particle Image Velocimetry (PIV) to improve the induced flow velocity measurements. A high speed PIV will be able to accurately record the induced pulsed wall jet profiles. In conjuction with the velocity measurements the effects of the RailPAc on the aerodynamic forces will be measured on the load beams that secure the test article to the wind tunnel. The changes in lift and drag will show the magnitude of the force created by the RailPAc on the airfoil.

Additional future plans include experiments to gain a detailed understanding of the improvements to the static stall angle, the optimal actuator geometry, excitation duty cycle, and behavior of the plasma armature at high Mach/Reynolds number. Finally, an exstensive material study will be conducted to determine the best metal or composite material required for optimal plasma armature performance.

Bibliography

[1] Leishman, J.G., *Principles of Helicopter Aerodynamics*, Cambridge University Press, New York, NY 2002, pp. 27, 380-381.

[2] Carr, L. W., and McAlister, K.. W., "The Effect of a Leading Edge Slat on the Dynamic Stall of an Oscillating Airfoil," Paper AIAA 83-2533, AIAA/AFS Aircraft Design, Systems, and Operations Meeting, Ft. Worth, TX, Oct. 1983.

[3] Yu, Y.H., McAlister, K. W., Tung, C., and Wang, C. M., "Dynamic Stall Control for Advanced Rotorcraft Application," *AIAA Journal*, Vol. 33, (2), Feb. 1992, pp. 289-295.

[4] Karim, M. A. and Achyara, M., "Control of the Dynamic Stall Vortex over a Pitching Airfoil by Leading Edge Suction," Paper AIAA 93-3267, Shear Flow Conference, Orlando, FL, July 1993.

[5] Lorber, P., McCormick, D., Anderson, T., Wake, B., MacMartin, D., Pollack, M., Corke, T., Breuer, K., "Rotorcraft Retreating Blade Stall Control," Paper AIAA 2000-2475, Fluids 2000 Conference and Exhibit, Denver, CO, June 2000.

[6] Yeo, H., "Assessment of Active Controls for Rotor Performance Enhancement," *Journal of the American Helicopter Society*, Vol. 53, (2), Apr. 2008, pp. 152-163.

[7] Suzen, Y. B., and Huang, P. G., "Simulations of Flow Separation Control Using Plasma Actuators." Paper AIAA 2006-877, Aerospace Sciences Meeting and Exhibit, Reno, NV, Jan. 2006.

[8] Moreau, E., "Airflow Control by Non-Thermal Plasma Actuators," *Journal of Physics D: Applied Physics*, Vol. 40, (3), 2007, pp. 605-636.

[9] Post, M. L., and Corke, T. C., "Separation Control on a High Angle of Attack Airfoil Using Plasma Actuators," *AIAA Journal*, Vol. 42, 11, 2004, pp. 2177-2184.

[10] Enloe, C.L., McLaughlin, T.E. , VanDyken, R.D. , Kachner, , Jumper, E.J., and Corke, T.C. , "Mechanisms and responses of a single dielectric barrier plasma actuator: Plasma morphology," *AIAA Journal,* Vol. 42, 3, 2004, pp. 589–594.

[11] Santhanakrishnan, A., and Jacob, J. D., "Flow Control With Plasma Synthetic Jet Actuators," *Journal of Physics D: Applied Physics*, Vol. 40, (3), 2007, pp. 637-651.

[12] Post, M. L., and Corke, T. C., "Seperation Control Using Plasma Actuators-Dynamic Stall Vortex Control on an Oscillating Airfoil," *AIAA Journal*, Vol. 44, (12), 2006, pp. 3125-3135.

[13] Nelson, R. C., Corke, T. C., and Othman, H., "A Smart Wind Turbine Blade Using Distributed Plasma Actuators for Improved Performance," Paper AIAA 2008-1312, 46th Aerospace Sciences Meeting, Reno, NV, Jan. 2008.

[14] Patel, M. P., Ng, T. T., Vasudevan S., Corke, T. C., and He, C., "Plasma Actuators for Hingless Aerodynamic Control of an Unmanned Air Vehicle," *Journal of Aircraft*, Vol. 44, (4), Aug. 2007, pp. 1264-1274.

[15] Patel, M. P., Ng, T. T., Vasudevan S., Corke, T. C., Post, M. L., McLaughlin, T. E., and Suchomel, C. F., "Scalling Effects of an Aerodynamic Actuator," *Journal of Aircraft*, Vol. 45, (1), 2008, pp. 223-236.

[16] Pai, S. T., and Zhang, Q., "Introduction to High Power Pulse Technology," *Advance Series in Electrical and Computer Engineering*, Vol. 10, 1995, pp. 272-274.

[17] Kelkar, M., and Heberlein, J., "Physics of an Arc in Cross Flow," *Journal of Applied Physics*, Vol. 33, 2000, pp. 2177.

Vita

Brent Pafford was born in Ruidoso, NM on 24 April 1982, the son of Joel and Joelyn Pafford. He received a Bachelor of Science degree in Aerospace Engineering from the United States Military Academy at West Point, NY. Before starting Graduate School, Brent Pafford served as an Aviator in the United States Army. Brent's research interests include:

- Aerodynamic flow control
- Rotorcraft design
- Aero elasticity

This thesis was typed by the author.

Electronic mail address: brent.pafford@utexas.edu